CHAPTETR 3

Materials and methods

In this chapter, the experimental procedures for preparation and characterization of powders and ceramics were presented. The characterization techniques were used to investigate microstructure, phase evolution, physical properties, dielectric and ferroelectric properties were presented in details as the following sections. The details are presented in the following sections.

3.1 Sample preparation

The sample fabrication in this work was divided into two parts: powder and ceramic preparations. The details of each part are given as follows.

3.1.1 Powder preparation

Compound powders of $Ba_{0.85}Ca_{0.15}Zr_{0.1}Ti_{0.9}O_3$ (BCZT) were synthesized by sol-gel auto combustion method [58] using barium nitrate ($Ba(NO_3)_2$) (99.0%, Himedia), calcium nitrate ($Ca(NO_3)_2{\cdot}4H_2O$) (99.0%, Sigma Aldrich), zirconium nitrate ($Zr(NO_3)_4{\cdot}3H_2O$) (99.0%, Sigma Aldrich), titanium (IV) butoxide ($(C_4H_9O)_4Ti$) (97.0%, Sigma Aldrich) and citric acid ($C_6H_8O_7$) (99.5%, Sigma Aldrich) as precursors. Predetermined amounts of $Ba(NO_3)_2$ and $Ca(NO_3)_2{\cdot}4H_2O$, $Zr(NO_3)_4{\cdot}3H_2O$ were mixed with 100 ml deionized (DI) water in a beaker as solution A. Then, $C_6H_8O_7$ and $(C_4H_9O)_4Ti$ were mixed in a beaker as solution B. The mixture was stirred while heated at 70°C. The pH value of the mixture was adjusted to 7 by slight NH_4OH. When adding the solution B became transparent, it was then added into the solution A while the mixture was still being stirred. After that, NH_4OH was added into the solution to adjust the pH value from 5 to 9. The temperature of the stirred-solution was increased up to 200 ºC until the solution became black powder, so-called “as-burnt powder”. The as-burnt powder was investigated by DTA/TG to determine the calcination temperature. As-burnt powders were calcined at 700-1000°C for soaking time of 2 h. The heating profile for the calcination is as shown in

Fig. 3.1. Phase of as-burnt and calcined powders was characterized using an X-ray diffractometer (X' Pert Phillips) with CuK_{α} radiation (λ = 1.54178 Å) at 2θ range of 20-80°. Chemical-bond vibrational spectras were observed by Fourier transform infrared spectrometer (FTIR, 510, Nicolet, America). The vibration and rotation of molecular structure for other frequencies were characterized by Raman spectroscopy (T 64000) in a range of 400-4000 cm^{-1}. Microstructure was observed by a transmission electron microscope (TEM: JSM-2010) and a scanning electron microscope (SEM: JEOL JSM-6335F). The flow chart of BCZT powder preparation is illustrated in Fig. 3.2. All commercially available starting materials which were used in this work are listed in Table 3.1, along with their supplier names formula weights and purities.

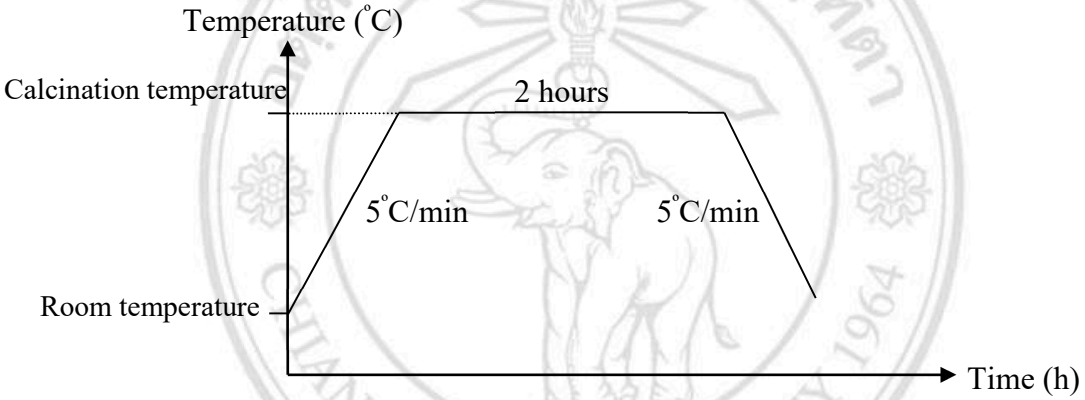

Figure 3.1 A diagram of the calcination process for $Ba_{0.85}Ca_{0.15}Zr_{0.1}Ti_{0.9}O_3$ powder at various temperatures.

Table 3.1 Specifications of the materials used in this work.

Material	**Source**	**Formula weight**	**Purity (%)**
$Ba(NO_3)_2$ (powder)	Himedia	261.33	99.0
$Ca(NO_3)_2 \cdot 4H_2O$ (powder)	Sigma Aldrich	236.14	99.0
$Zr(NO_3)_4 \cdot 3H_2O$ (powder)	Sigma Aldrich	393.28	99.0
$(C_4H_9O)_4Ti$ (solution)	Sigma Aldrich	340.32	97.0
$C_6H_8O_7$ (powder)	Sigma Aldrich	192.12	99.5
Bi_2O_3 (powder)	Fluka	465.96	98.0
$69Pb(Mg_{1/3}Nb_{2/3})O_3$–$31PbTiO_3$ crystal (PMN-PT) (solid)	IBULE PHOTONICS, Incheon, Korea		

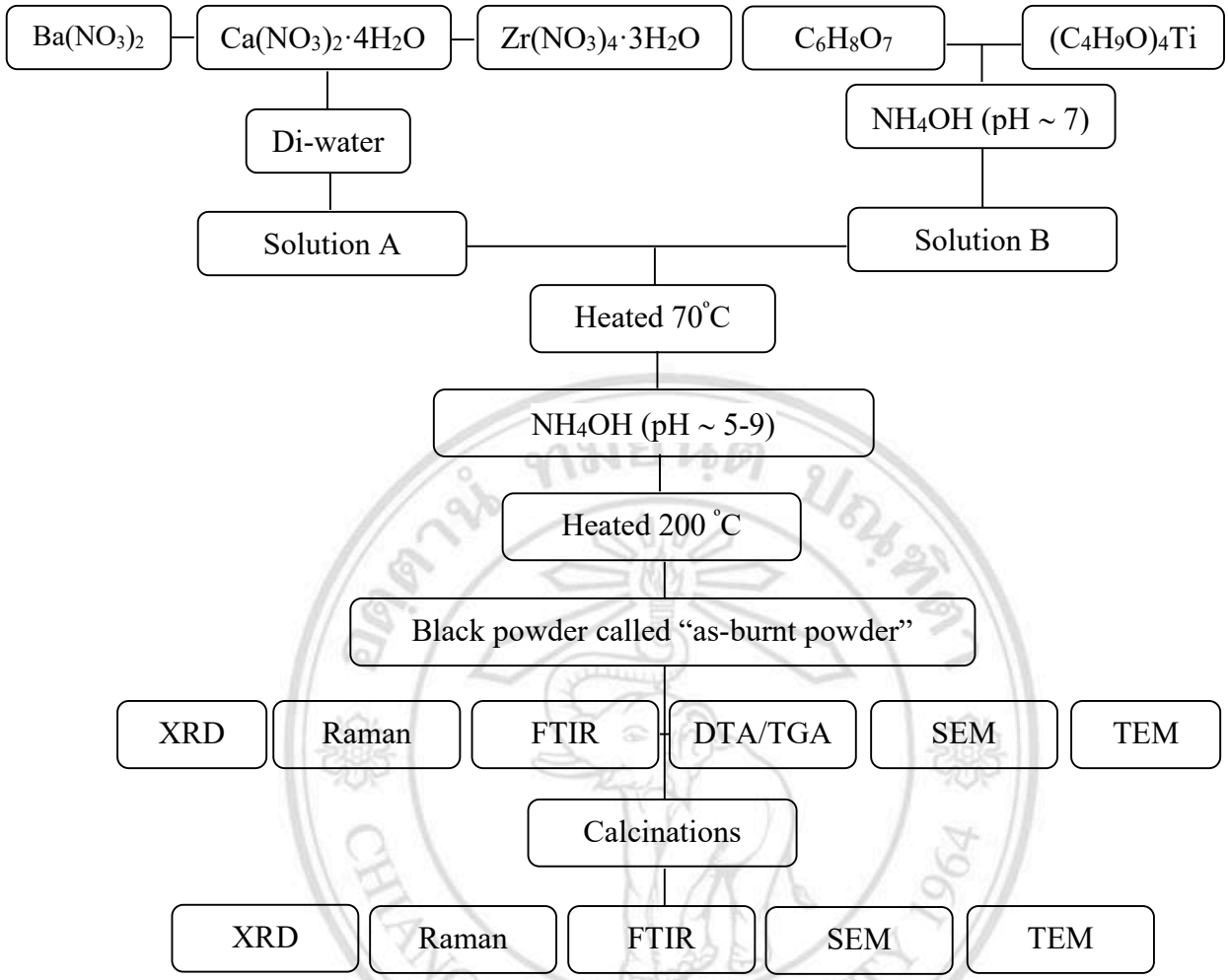

Figure 3.2 Preparation diagram for BCZT powders derived by sol-gel auto combustion.

3.1.2 Ceramic preparation

In this section, preparations all ceramic systems have been carried out using a solid state sintering method. Each system of powders and ceramics were prepared and discribed in details.

3.1.2.1 BCZT system

BCZT calcined powders were remixed by ball milling method in ethanol medium for 24 h. After that, the mixed powders were dried. For each sample, the powders were weighted for 0.75 g and pressed under pressure 1 ton for 15 seconds to prepare pellets with a

diameter of 10 mm. The pellets were placed on an alumina plate covered by an alumina lid. Top and side views of sample arrangement are presented in Fig. 3.3(a) and (b), respectively. The samples were sintered at 1200-1500°C with a soaking time of 2 h with a heating rate of 5°C/min. A temperature profile for sintering process of the samples is displayed in Fig. 3.4. A schematic diagram of the BCZT ceramic preparation is illustrated in Fig. 3.5.

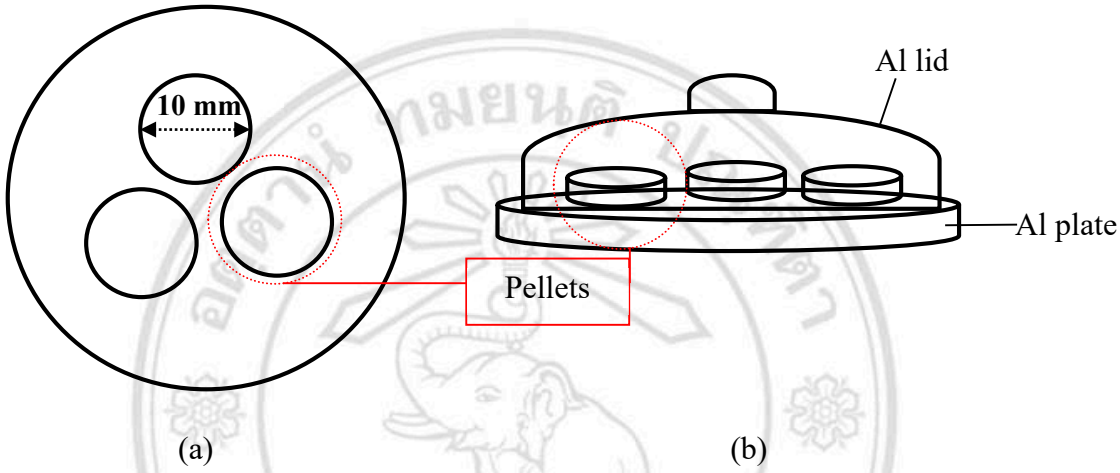

Figure 3.3 The pellet arrangement for the sintering process of the ceramics : (a) top viea and (b) sid view.

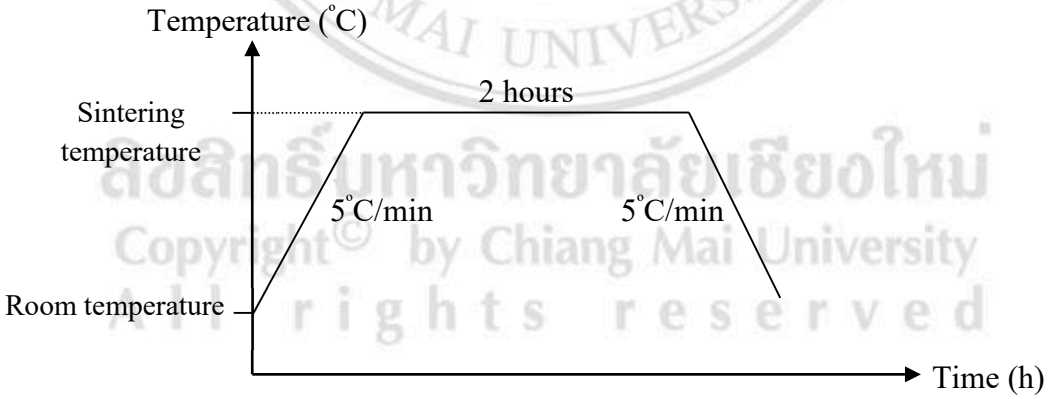

Figure 3.4 A Diagram of a sintering process of $Ba_{0.85}Ca_{0.15}Zr_{0.1}Ti_{0.9}O_3$ ceramics at various temperatures.

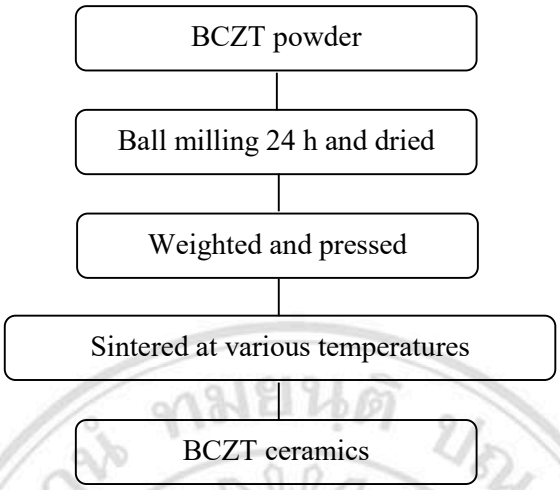

Figure 3.5 A diagram for BCZT ceramics preparation at various temperatures.

3.1.2.2 BCZT-*x*Bi system

Different amounts of Bi_2O_3 powders, *0.005, 0.01, 0.015, 0.02, 0.03, 0.1* mole fraction (namely BCZT-*0.005*Bi, BCZT-*0.01*Bi, BCZT-*0.015*Bi, BCZT-*0.02*Bi, BCZT-*0.03*Bi and BCZT-*0.1*Bi) were added into BCZT calcined powders. These powders were mixed by ball milling for 24 h by using ethanol as a medium. After that, the mixed powders were dried in an oven for 24 h to form BCZT-*x*Bi powders. The BCZT-*x*Bi powders were weighed (0.7500 g) and pressed under a pressure of 1 ton for 15 seconds to form pellets with a diameter of 10 mm. The pellets were placed on an alumina plate covered by an alumina lid and sintered at 1000, 1050, 1100, 1150 and 1200°C with soaking time of 2 h. A sintering profile and a BCZT-*x*Bi ceramics preparation procedure are displayed in Fig. 3.6 and Fig. 3.7, respectively.

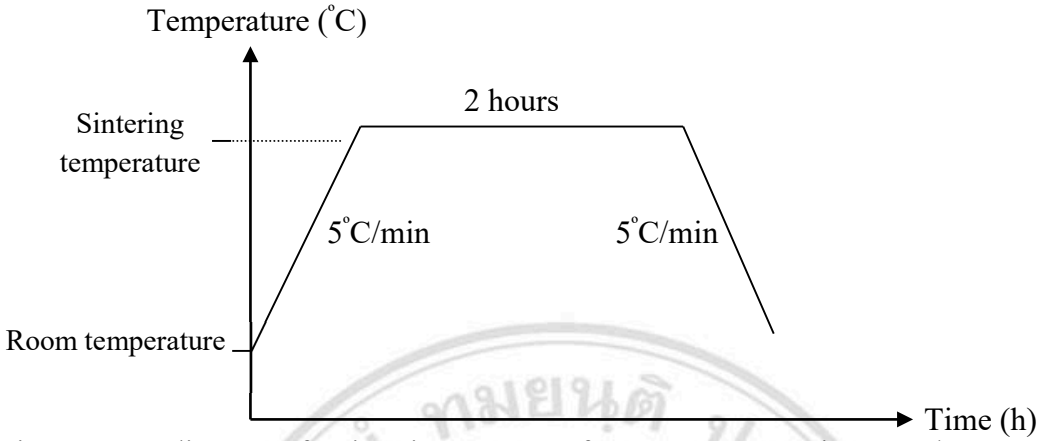

Figure 3.6 A diagram of a sintering process of $Ba_{0.85}Ca_{0.15}Zr_{0.1}Ti_{0.9}O_3$-$xBi_2O_3$ ceramics at various temperatures.

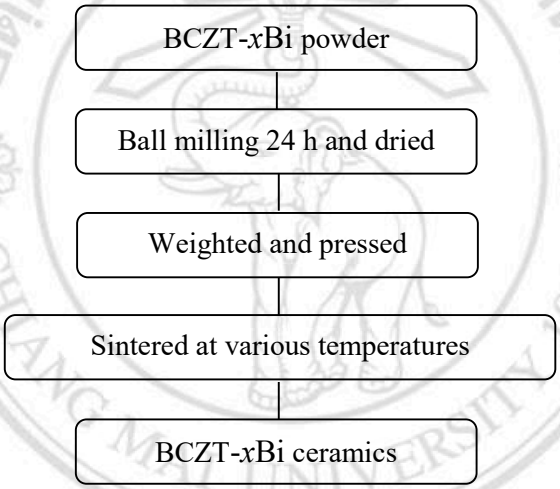

Figure 3.7 A preparation diagram for $Ba_{0.85}Ca_{0.15}Zr_{0.1}Ti_{0.9}O_3$-$xBi_2O_3$ ceramic at various temperatures.

According to the results of BCZT ceramic preparations and variation of Bi_2O_3 content, the sintering temperatures at 1200°C with Bi_2O_3 content of *0.02* mole fraction was an optimum condition. Then, the effect of sintering time was with also investigated. The green samples were sintered at 1200°C with soaking times of 2, 5, 10 and 15 h with a heating rate of 5°C/ min. A heating profile for the sintering procedure is shown in Fig. 3.8.

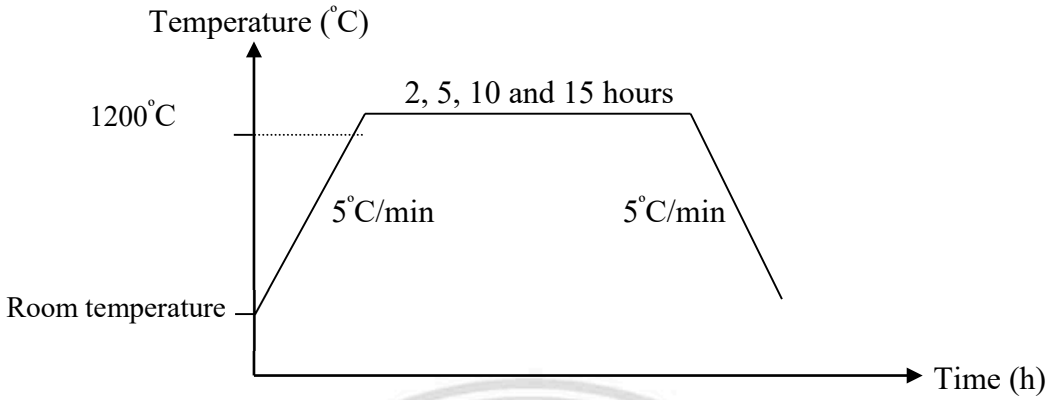

Figure 3.8 A diagram of a sintering process of $Ba_{0.85}Ca_{0.15}Zr_{0.1}Ti_{0.9}O_3$-*0.02*$Bi_2O_3$ ceramics at 1200°C with different sintering times.

3.1.3 BCZT-0.02Bi-xPMNT system

After obtaining the optimized sintering condition for BCZT-0.02Bi ceramics, BCZT-0.02Bi powders were mixed with different amounts of 69Pb($Mg_{1/3}Nb_{2/3}$)O_3-31$PbTiO_3$ (PMN-PT) crystals to form BCZT-0.02Bi-*x*PMNT composition where *x* = 1, 3 and 5 weight fractions (abbreviated as BCZT-*0.02*Bi, 1PMNT, 3PMNT and 5PMNT, respectively). The size of the PMNT crystals was 0.7x1.0x1.0 mm^3. The BCZT-0.02Bi-*x*PMNT mixtures were manually ground and pressed into pellets under 1 ton pressure for 15 seconds. The schematic preparation diagram of BCZT-0.02Bi-*x*PMNT pellets is displayed in Fig. 3.9. The diagrams of the sintering procedure and the whole process for the preparation of the BCZT-0.02Bi-*x*PMNT ceramics are shown in Fig. 3.10 and Fig. 3.11, respectively.

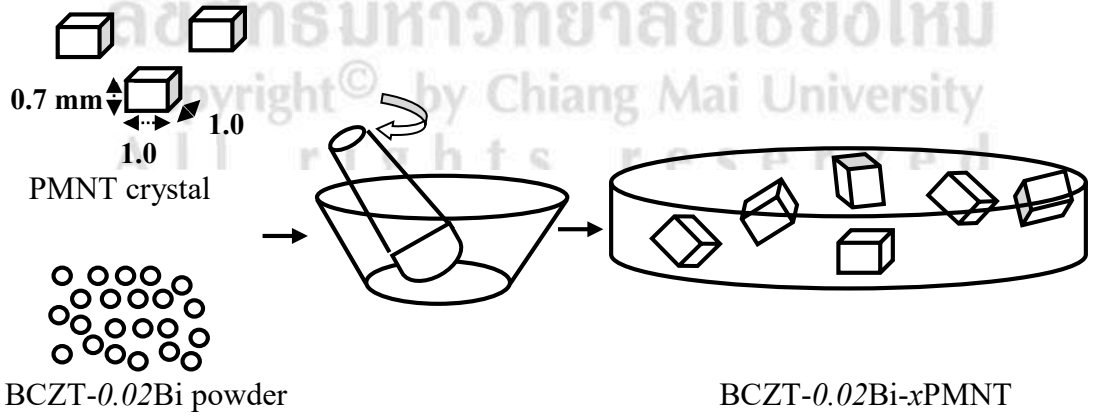

Figure 3.9 Schematic diagram of BCZT-*0.02*Bi-*x*PMNT sample preparation.

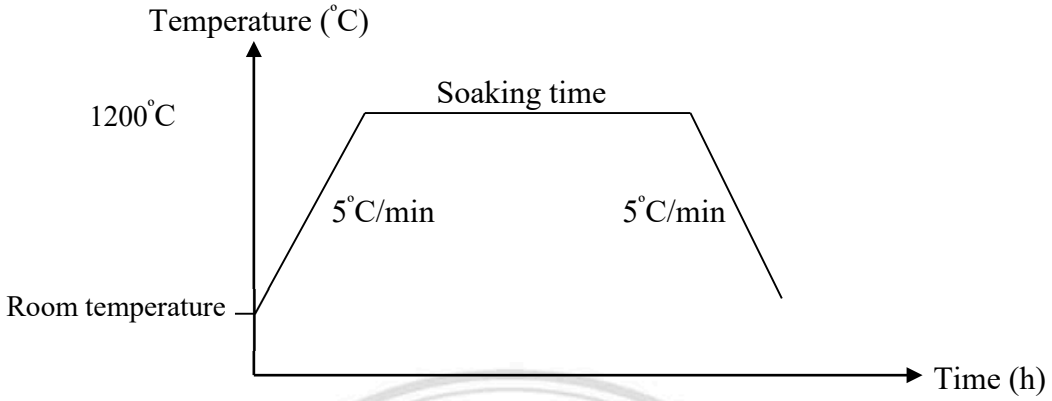

Figure 3.10 A diagram of a sintering process of BCZT-*0.02*Bi-*x*PMNT ceramics.

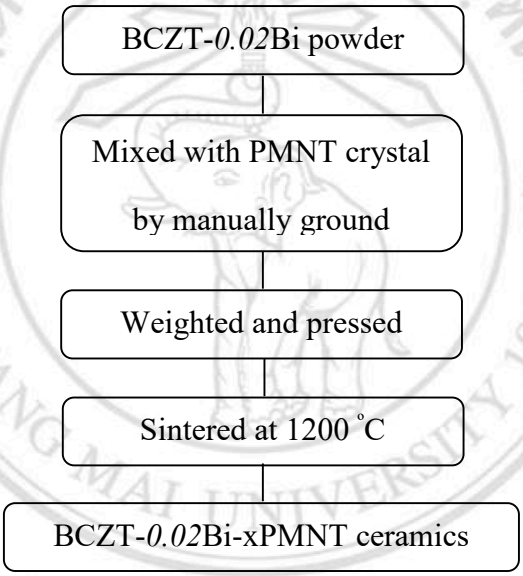

Figure 3.11 A diagram of the preparation of BCZT-*0.02*Bi-*x*PMNT ceramics.

3.2 Sample characterization

All prepared samples were characterized in terms of phase formation, vibration and rotation of molecular structure, chemical bonding vibration, density, weight loss, crystal structure, microstructure, dielectric and ferroelectric properties as described in the following sections.

3.2.1 Thermal analysis

Thermal analysis of as-burnt powders was characterized by differential scanning calorimeter (DSC) and thermo-gravimetric (TG) methods. In this work, the DSC apparatus [NETZSCH STA (Model No 409C)], as shown in Fig. 3.12, with a heating rate of 10ºC/min in the N_2 atmosphere was used. DSC/TG provides the data about the decomposition and crystallization of the as-burnt powders. The DSC/TG characterization was performed at the temperature ranged from room temperature to 1000ºC.

Figure 3.12 A differential scanning calorimeter [NETZSCH STA (Model No 409C)].

3.2.2 Raman spectra analysis

Vibration and rotation of molecular structures at different frequencies were characterized by the Raman spectroscopy technique (T 64000) in a range of 400–4000 cm^{-1} at room temperature. After a sample was bombarded by a monochromatic light, the phonons inside the sample were observed which caused the energy to shift up and down from phonon modes. Raman scattering has been used for studying the phase formation of as-burnt powers and its dependence on different calcination temperatures. A raman spectrometer is shown in Fig.3.13.

Figure 3.13 A raman spectrometer (T64000).

3.2.3 Fourier transform infrared spectroscopic analysis

Chemical-bond vibration with various frequencies and structure evolution of as-burnt powders and calcined powders were studied by a Fourier transform infrared spectrometer (FTIR, Bruker; Model Tensor 27) as shown in Fig. 3.14. After a sample was detected by infrared light (IR) the data was observed from the molecular vibration at the same frequency of IR.

Figure 3.14 A fourier transform infrared spectrometer (Model Tensor 27).

3.2.4 X-ray diffraction analysis

Phase formation of samples was characterized by an X-ray diffractometer (XRD, X' Pert MPD Phillips), as shown in Fig. 3.15. The CuK_{α} radiation with wavelength of 1.5405 Å was used as XRD source. The diffractometer was operated with a current of 35 mA and

voltage of 40 kV. XRD data at 2θ ranged from 20º to 80º was recorded with a step size of 0.02º.

Figure 3.15 an X-ray diffractometer.

When the X-ray beam from the XRD source is incident on the sample, it is partly absorbed, transmitted and scattered. The scattering of X-ray is related to the interaction between the electromagnetic wave and crystal lattices of the sample. The different lattices interfere with each other to produce scattered X-ray with a different patterns and it depends on a change of incident angle. The X-ray measurement configuration is consisted of an incident X-ray beam impinging on the surface of sample and then the beam diffracted at the same angle is detected. The XRD peak will appear when Bragg's law is satisfied as shown in Fig.3.16. The formula of Bragg's law is

$$2d \sin\theta = n\lambda \qquad (3.1)$$

where d is the interplanar spacing of the crystal,

θ is a Bragg angle,

n is an integer order of a diffraction peak,

λ is the wavelength of an X-ray.

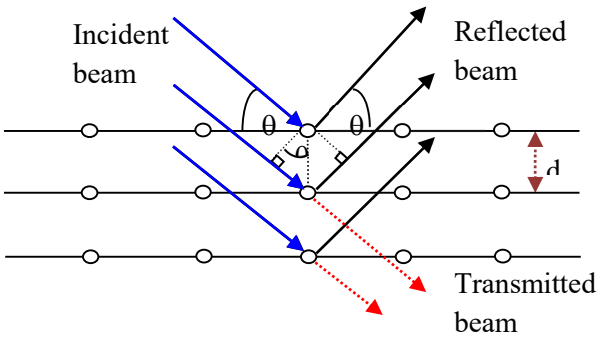

Figure 3.16 A schematic diagram of Bragg's law reflection.

3.2.5 Crystal structure

In this work, the crystal structure of all samples was defined using Powder Cell software. This program was introduced by W. Kraus and G. Nolze [61] for identifying the crystal structure of the samples. Firstly, all parameters of crystal structure such as lattice parameters, space group and atomic position were filled in the program. The above parameters could be changed. Then, the program generated those parameters and simulated patterns. For good fitting, chi-square (χ^2) should be close to 1 [62]. A software screen and a final simulated pattern are illustrated in Fig.3.17.

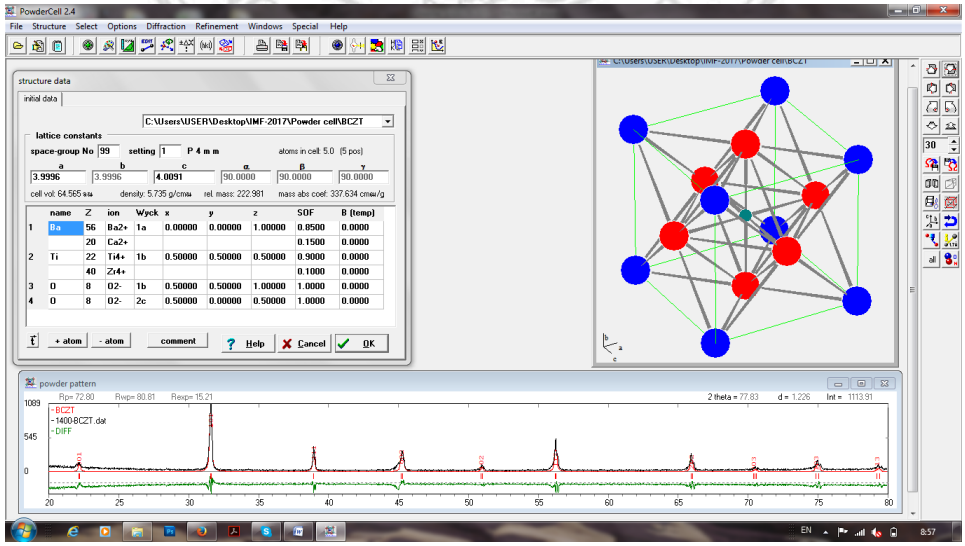

Figure 3.17 A feature of Powder Cell program with all refined parameters, crystal structure and simulated pattern.

3.2.6 Physical property measurement

Physical properties such as density, shrinkage and weight loss of samples were studied. Archimedes' equation was used to calculate densities of samples. Firstly, a weight of a dried sample was weighted and recorded as W_1. The sample was boiled in water for 4 hours and continuously kept in the distilled water for 24 hours. The weight of the sample was then measured as W_2. Finally, the sample was weighed while being immersed in water and recorded as W_3. All parameters (W_1, W_2 and W_3) were employed to calculate the density of the sample by using the following equation,

$$\rho = \left(\frac{W_1}{W_2 - W_3} \right) x \rho_{water} \tag{3.2}$$

where ρ_{water} is the density of water in g/cm^3, which weakly depends on temperature, i.e.

$$\rho_{water} = 1.0017\text{-}0.0002315\ T \tag{3.3}$$

where T is the temperature of water in ºC.

The shrinkage and weight loss of all samples were calculated from the diameter and weight before sintering, represented by d_1 and w_1, respectively, and those after sintering, represented by d_2 and w_2, respectively. Shrinkage and weight loss can be calculated by using the following equations (3.4) and (3.5), respectively.

$$\text{Shrinkage (\%)} = \left(\frac{d_2 - d_1}{d_1} \right) x100 \tag{3.4}$$

$$\text{Weight loss (\%)} = \left(\frac{W_2 - W_1}{W_1} \right) x100 \tag{3.5}$$

3.2.7 Microstructure analysis

Scanning electron microscopy (SEM) and transmission electron microscopy (TEM) are very popular techniques for characterization of microstructure at high magnification.

Electrons generated from a tungsten-hairpin filament (LaB_6) or a field emission gun are accelerated and focused onto a sample as shown in Fig. 3.18. SEM images can be formed by two interesting signals, i.e. backscattered and secondary electrons. Images may be obtained from these two signals as well as electron diffraction spots and high resolution image from transmitted beam impinging on the film as TEM detector.

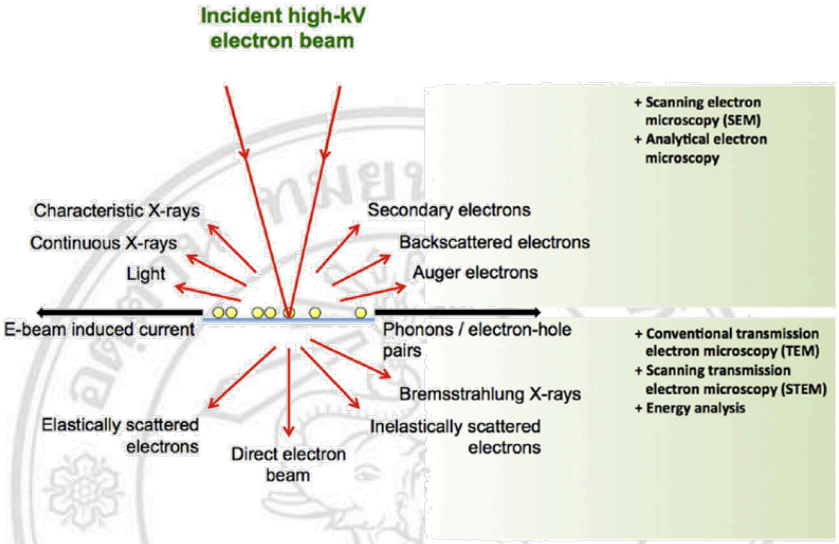

Figure 3.18 A schematic illustration of the interaction between an incident electron beam and a sample [63].

In this work, a scanning electron microscope (SEM, JEOL JSM-6335F, Japan and SEM, JSM-IT300LV), as shown in Fig. 3.19 and Fig. 3.20, were used to determine morphologies of as-burnt powders, calcined powders and ceramics 's surfaces. As-burnt powders and calcined powders were dispersed in ethanol medium by using an ultrasonic vibrator. The powders were then dropped on a copper tape and coated with gold using a sputter coater (JFC-1100E), as shown in Fig.3.21. For ceramic samples, after polishing they were cleaned using ultrasonic cleaner and also coated with gold film. A linear interception method was used to determine grain sizes of ceramics from SEM images.

Figure 3.19 A scanning electron microscope (SEM, JEOL JSM-6335F).

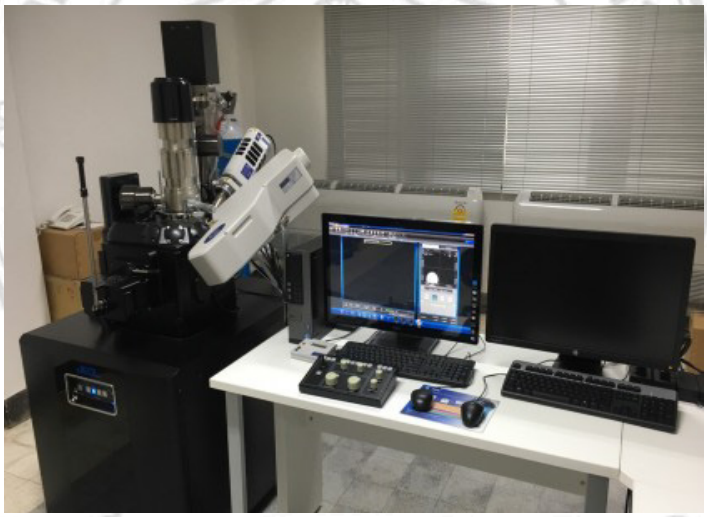

Figure 3.20 A scanning electron microscope (JSM-IT300LV).

Figure 3.21 A sputter coater (JFC-1100E).

In this work, as-burnt and calcined powders were characterized using a transmission electron microscope (TEM, JEOL JSM-2010, Japan), as shown in Fig.3.22. All powders were prepared by dispersing in an ethanol using ultrasonic vibrator. Then the slurry was dropped on the copper grid and dried.

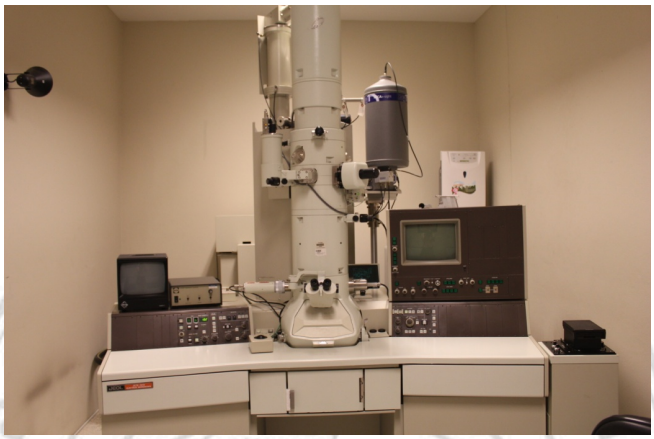

Figure 3.22 A transmission electron microscope (TEM, JEOL JSM-2010).

3.2.8 Dielectric property analysis

In this work, temperature dependence of dielectric properties, i.e. dielectric permittivity and dielectric loss, were measured at different frequencies by an Alpha high resolution dielectric/impedance analyzer (NovoControl) or Solartron 1260 impedance analyzer combined with a Solartron 1296 dielectric interface as shown in Fig. 3.23. The samples were prepared by polishing both parallel surfaces by SiC paper under cooling by water. The thickness of all samples was ~ 1 mm for dielectric measurement. The samples surfaces were cleaned using an ultrasonic bath and dried overnight at 150°C. The polished surfaces of samples were painted by silver paste as electrodes and fired at 550°C for 15 min. After that, an electrode sample was placed in the holder of the dielectric analyzer. The properties were measured from -100°C to 300°C with heating rate of 5°C/minutes. The measurement frequency was from 100 Hz to 1 MHz.

A capacitance (C) of a dielectric material can be calculated by the following formula,

$$C = \varepsilon_r \varepsilon_0 \left(\frac{A}{d} \right) \tag{3.6}$$

where ε_0 is the permittivity of vacuum, 8.854×10^{-12} F/m

ε_r is the dielectric permittivity of the material

A is the electrode area of the material

d is the thickness of the material.

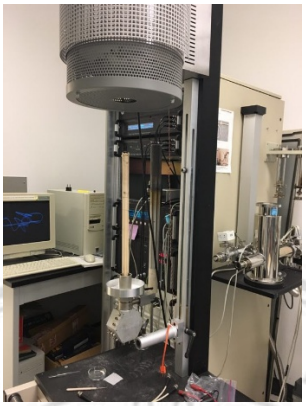

Figure 3.23 An alpha high resolution dielectric/impedance analyzer (NovoControl) or Solartron 1260 impedance analyzer combined with a Solartron 1296 dielectric interface.

3.2.9 Ferroelectric property analysis

Ferroelectric properties of all samples were characterized by a Ferroelectric a Radiant RT-66 standardized ferroelectric testing system, as shown in Fig. 3.24 which could give electric field dependences of polarizations (P) calculated by dividing charges (Q) with area of sample (A) as defined below:

$$P = \frac{Q}{A} \tag{3.7}$$

Figure 3.4 shows a modified Sawyer-Tower circuit for the measurement of ferroelectric hysteresis loops [64], where C_s, R_s, C_r, R, V, *and* V_r stand for the capacitance of the sample, the resistance of the sample, the capacitance of the reference capacitor, the resistor, the applied voltage, and the voltage across the reference capacitor, respectively.

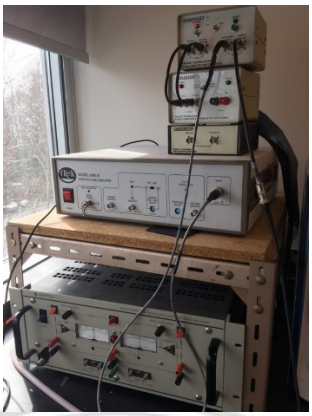

Figure 3.24 A Radiant RT-66 standardized ferroelectric testing system.

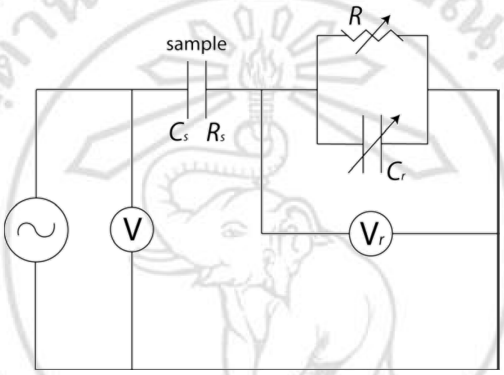

Figure 3.25 A modified Sawyer-Tower circuit for the measurement of ferroelectric

In this circuit, a voltage (V) was applied across the electrodes of a material (C_s, with thickness t). An electric field was determined from the voltage divided by the sample thickness ($E=V/t$). The field applied was plotted on the x-axis. Then, the material was connected in series with a parallel RC circuit which compensates for any phase shift related to conductivity or dielectric loss in the material. The voltage (V_r) across the reference capacitor (C_r) was measured. The charge on the ferroelectric material can be determined from multiplying V_r with Q_r.

3.2.10 Electrostrictive measurement

Electrostrictive properties of samples were obtained using a strain sensor in conjunction with a high voltage source at which strain-electric field (S-E) curves were displayed. Figure 3.26 presents an electrostrictive measurement apparatus. Bipolar electric field was applied accross both electrodes of a sample and the induced strain was observed by the strain sensor.

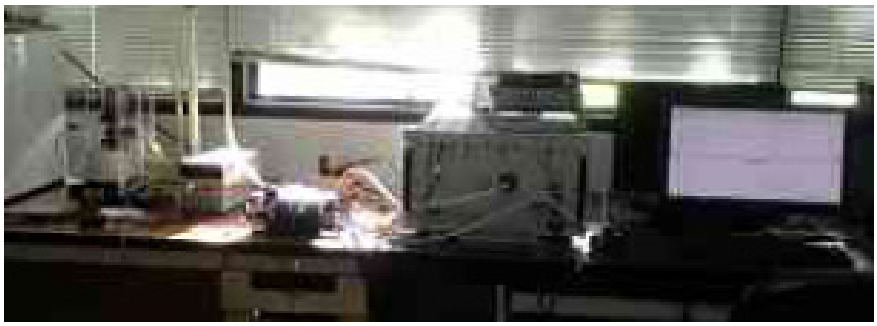

Figure 3.26 An electrostrictive measurement apparatus.